In situ spectroscopic ellipsometry study on the growth of ultrathin TiN films by plasma-assisted atomic layer deposition

In situ spectroscopic ellipsometry study on the growth of ultrathin TiN films by plasma-assisted atomic layer deposition

E. Langereis,[a] S. B. S. Heil, M. C. M. van de Sanden, and W. M. M. Kessels[b]
Department of Applied Physics, Eindhoven University of Technology, P.O. Box 513, 5600 MB Eindhoven, The Netherlands

(Received 6 March 2006; accepted 12 May 2006; published online 31 July 2006)

The growth of ultrathin TiN films by plasma-assisted atomic layer deposition (PA-ALD) was studied by *in situ* spectroscopic ellipsometry (SE). In between the growth cycles consisting of $TiCl_4$ precursor dosing and H_2–N_2 plasma exposure, ellipsometry data were acquired in the photon energy range of 0.75–5.0 eV. The dielectric function of the TiN films was modeled by a Drude-Lorentz oscillator parametrization, and the film thickness and the TiN material properties, such as conduction electron density, electron mean free path, electrical resistivity, and mass density, were determined. *Ex situ* analysis was used to validate the results obtained by *in situ* SE. From the *in situ* spectroscopic ellipsometry data several aspects related to thin film growth by ALD were addressed. A decrease in film resistivity with deposition temperature between 100 and 400 °C was attributed to the increase in electron mean free path due to a lower level of impurities incorporated into the films at higher temperatures. A change in resistivity and electron mean free path was observed as a function of film thickness (2–65 nm) and was related to an increase in electron-sidewall scattering for decreasing film thickness. The TiN film nucleation was studied on thermal oxide covered *c*-Si substrates. A difference in nucleation delay was observed on these substrates and was related to the varying surface hydroxyl density. For PA-ALD on H-terminated *c*-Si substrates, the formation of an interfacial SiN_x film was observed, which facilitated the TiN film nucleation. © *2006 American Institute of Physics*. [DOI: 10.1063/1.2214438]

I. INTRODUCTION

Atomic layer deposition (ALD) has recently gained a lot of interest in research and development due to its intrinsic growth control by the virtue of self-limited surface reactions.[1–4] The characteristic layer-by-layer growth, excellent uniformity, and ultimate conformality in high-aspect ratio features make ALD a promising technique to deposit ultrathin films in integrated circuits.[1] In the literature, many ALD schemes are reported to achieve layer-by-layer growth of a large variety of materials.[2,4] In addition, the plasma-assisted atomic layer deposition (PA-ALD) technique is believed to offer the same advantages as ALD as well as a larger freedom in materials and processes, improved material quality, and lower deposition temperature.[5–7]

When reducing the film dimensions towards the nanometer scale, detailed insight into aspects such as finite size effects, film nucleation, and interface formation/modification becomes essential.[8–11] Therefore, successful application of ultrathin films in devices has to be accompanied by accurate metrology techniques to determine the properties of these thin films. The films are mostly studied by *ex situ* diagnostics giving detailed insight into the thin film properties, however, at the cost of time-consuming and often sample-destructive procedures. For example, Satta *et al.* reported on the ALD film growth process using elaborate Rutherford backscattering spectroscopy,[9] but the analysis required separate samples for each condition and film thickness that was examined. Furthermore, for materials that are air sensitive, an *ex situ* measurement could result in different material properties due to the exposure of the films to the ambient.

A detailed understanding of the growth process and material properties of the ultrathin films can be obtained by the application of *in situ* diagnostics. In the literature, several *in situ* studies on ALD-deposited thin films have been reported using diagnostics such as quartz crystal microbalance measurements,[12,13] x-ray diffraction spectroscopy,[14] and infrared spectroscopy.[15,16] In this paper, we will present an *in situ* study of ALD thin film growth using the optical, nonintrusive technique of spectroscopic ellipsometry (SE), which can give insight into both the film thickness and the film properties of the thin films.

Several aspects of ultrathin film growth can be addressed by monitoring the process with spectroscopic ellipsometry. Ellipsometry is an accurate diagnostic to determine the thickness of the deposited layer. It is fast and nondestructive and can be used on wafer, which enables the *in situ* determination of the film thickness and, consequently, the growth rate of the process. The high sensitivity of ellipsometry (~0.01 monolayer) can also be used to study the film nucleation at the early stages of growth.[17] For many ALD processes, a distinct nucleation delay is observed due to the limited density of nucleation sites on the substrate surface.[9,16] Therefore, an understanding of the film nucleation is indispensable to know the film thickness after a certain number of cycles. Another important aspect which is closely related to initial film growth is substrate modification and interface layer for-

[a]Electronic mail: e.langereis@tue.nl
[b]Author to whom correspondence should be addressed; electronic mail: w.m.m.kessels@tue.nl

mation which can take place during the deposition process. Especially for applications relying on interface properties or based on a nanolaminate stack of films, the oxidation or nitridation of the underlying material during film growth could affect the aimed device structure and, thereby, deteriorate the device performance.[10,18] Because ellipsometry is sensitive to the optical constants of a material, it can be used to monitor the formation of an interfacial film given that the optical contrast between the different layers is sufficient.

Secondly, from the dielectric function of the deposited film determined from the spectroscopic ellipsometry data, material properties such as refractive index and extinction or absorption coefficient can be extracted. In addition, for thin metal films or films with metallic behavior, also the electronic properties can be calculated. Following the classical theory of light dispersion, the Drude theory can be used to model the intraband absorption in the metallic film.[19,20] In an ideal metal with all electrons free, the unscreened plasma energy $\hbar\omega_{pu}$ is defined by the energy position where the real part of the dielectric function is zero:[19]

$$\hbar\omega_{pu} = \hbar\sqrt{\frac{Ne^2}{\varepsilon_0 m^*}}, \tag{1}$$

where $\hbar$ is Dirac's constant, N is the conduction electron density, e is the electron charge, ε_0 is the permittivity of free space, and m^* is the electron effective mass. From the unscreened plasma energy in combination with the Drude broadening of the absorption, material parameters such as conduction electron density, electron mean free path, electrical resistivity, and mass density can be calculated. Therefore, *in situ* spectroscopic ellipsometry can be used to probe the electronic properties of films obtained under different deposition conditions as well as the dependence of the electronic properties on the film thickness. The so-called size effects become increasingly important for the future application of ultrathin films. For instance, Steinhögl *et al.* showed for the application of copper in interconnects that the conductivity of the metal strongly depends on the dimensions. They reported that an increase in resistivity caused by size effects in narrow copper lines (<100 nm) cannot be avoided and will require design rule modification.[8] It is obvious that the change of material properties with film thickness is of key importance for ALD of ultrathin metallic films and should be studied in greater detail.

In addition to the work of Patsalas and Logothetidis who used spectroscopic ellipsometry to study dc reactive magnetron sputtered TiN films,[21,22] we will use *in situ* spectroscopic ellipsometry to obtain detailed information on the film thickness and the material properties during the PA-ALD growth process of ultrathin TiN films. The experimental procedure and ellipsometry data analysis procedure using the Drude-Lorentz oscillator parametrization will be described in more detail in Secs. II and III, respectively. The TiN film thickness and material properties determined by spectroscopic ellipsometry will be related to the results of *ex situ* diagnostics and aspects such as size effects, film nucleation, and interface layer formation during PA-ALD will be discussed in Sec. IV. The conclusions are given in Sec. V.

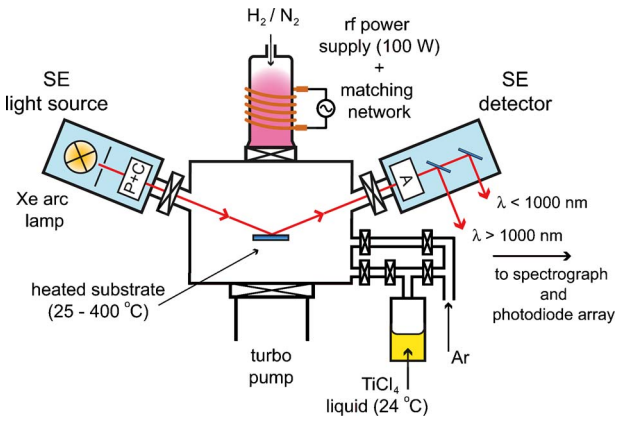

FIG. 1. (Color online) Schematic representation of the plasma-assisted atomic layer deposition system to deposit TiN films. The chamber is equipped with optical viewports to monitor the film growth *in situ* by spectroscopic ellipsometry.

II. EXPERIMENTAL SETUP

The thin TiN films were deposited by the PA-ALD technique using the deposition system schematically shown in Fig. 1 and that is described extensively in a previous publication.[6] Briefly, the system consists of a deposition chamber, a $TiCl_4$ dosing system, and plasma source, which are separated by pneumatic gate valves. The radio frequency plasma power (100 W) is coupled inductively to the plasma source which consists of a multiple-turn copper coil wrapped around a quartz tube. The wall-heated (~80 °C) deposition chamber contains a resistively heated substrate holder (25–400 °C). A PA-ALD cycle consists of 5 s of $TiCl_4$ exposure, followed by a 10 s purge with argon gas, subsequently 15 s plasma exposure, and 10 s pump down to base pressure (10^{-6} Torr). During $TiCl_4$ dosing the top and bottom pneumatic gate valves are closed and $TiCl_4$ vapor from a trapped volume is injected (Fig. 1). This leads to a pressure of 3 mTorr in the chamber during $TiCl_4$ dosing. The plasma is operated on H_2 and N_2 gas (10:1 ratio) at a total pressure of 11 mTorr.

The film growth was monitored by *in situ* SE using the optical viewports on the vacuum chamber (Fig. 1). The SE measurements were performed using a J.A. Woollam, Inc. M2000U visible and near-infrared rotating compensator ellipsometer (0.75–5.0 eV). The ellipsometer light source consists of a high pressure xenon arc lamp, a fixed polarizer (P), and rotating compensator (C) to define the polarization state of the light. After reflection on the substrate the polarization state of the light is determined by a fixed analyzer (A). In the detector, two mirrors split the reflected light into infrared and visible light, which is coupled via two optical fibers towards the spectrographs and photodiode arrays where the spectroscopic information of the reflected light is extracted. The angle of incidence was fixed to 68° with respect to the substrate normal and is close to the Brewster angle of silicon, which enlarges the sensitivity of *in situ* SE when measuring on silicon-based substrates.[23] The spot size on the substrate was ~5 mm in diameter. Pneumatic gate valves are present between the vacuum chamber and the optical windows to

prevent film deposition on the windows during the PA-ALD cycles.

The PA-ALD TiN films were deposited on different substrate materials. Depositions on native oxide covered *c*-Si substrates were used to determine typical material properties of the TiN film. The nucleation of TiN was studied on different silicon oxide substrates prepared by the method of calcination. The surface of the silicon oxides is covered with hydroxyl groups and siloxane bridges with the surface density of the hydroxyls mainly depending on the preheat temperature of the oxide.[24] Thermal oxides were prepared by heating *c*-Si substrates up to 750 °C (24 h, ~50 nm SiO_2) and 1000 °C (6 h, ~180 nm SiO_2) and the oxide surfaces are reported to have hydroxyl densities of 1–2 and 0–0.5 nm^{-2}, respectively.[24] The nucleation on these oxides was compared to the growth on a standard, as-received thermal silicon oxide wafer (~410 nm SiO_2 on *c*-Si). Furthermore, PA-ALD was studied on H-terminated *c*-Si substrates obtained by removal of the native oxide from a Si wafer with a 2% buffered HF solution.

The film properties obtained from the *in situ* SE data were compared to the properties obtained by *ex situ* diagnostics.[7] The film thickness and mass density were determined from x-ray reflectivity (XRR). The film stoichiometry and impurity content were determined by Rutherford backscattering spectroscopy (RBS), elastic recoil detection (ERD) analysis, and x-ray photoelectron spectroscopy (XPS). Four-point probe (FPP) measurements and x-ray diffraction (XRD) were used to determine the film resistivity and grain size, respectively.

III. SPECTROSCOPIC ELLIPSOMETRY

A. Data acquisition and optical model

After each PA-ALD cycle, spectroscopic data over the entire photon energy range were obtained by opening the gate valves to the ellipsometer light source and detector. To obtain a high signal to noise ratio in both the visible and the infrared part of the spectrum, each SE measurement consisted of the averaging of 500 data acquisitions leading to a measurement time of approximately 1 min. After the measurement, the gate valves were closed and the deposition process continued.

From model-based analysis of the ellipsometry data, the thickness of the film (for sufficiently thin films in the case of metallic films) as well as the optical constants can be extracted. The ellipsometry data can be expressed in terms of the pseudodielectric function $\langle\varepsilon\rangle$, which is represented in real $\langle\varepsilon_1\rangle$ and imaginary $\langle\varepsilon_2\rangle$ parts. Prior to the film deposition, the pseudodielectric function of the substrate was determined. For the H-terminated *c*-Si substrates, the pseudodielectric function was modeled with a semi-infinite silicon substrate which includes the substrate temperature dependence of the optical constants of silicon.[25] The substrate modeling of the native and thermal oxide substrates required an additional Cauchy layer to describe the contribution of the transparent oxide film to the pseudodielectric function of the substrate.[17]

The deposited TiN film was modeled by adding another layer on top of the substrate model. Assumptions within this approach are that the deposition process does not affect the substrate properties and that a surface roughness layer can be neglected. The latter assumption was validated by the low surface roughness (0.4 nm for a 12 nm film) observed by atomic force microscopy (AFM) measurements (see Sec. IV). In the present work, the modeling of the ellipsometry data was performed using the WVASE32 software for data analysis from J.A. Woollam.[26] The quality of the fit can be expressed by the mean squared error (MSE) between the experimental data and the model fit. The data fitting used a Levenberg-Marquardt algorithm to minimize the MSE.[17]

B. Dielectric function of TiN

1. Drude-Lorentz oscillator parametrization

The dielectric function of the TiN films can be modeled by a Drude-Lorentz oscillator parametrization.[21,22] The Drude oscillator accounts for the intraband absorption of the free electrons and, therefore, contains information on the metallic properties of the TiN film.[19] The interband absorptions in the TiN can be described by Lorentz oscillators.[21] In the literature, the dielectric function of TiN is often composed of two Lorentz oscillators to account for the interband absorption around 3.5 and 5.2 eV.[21,27,28] We adopted the same model and describe the dielectric function ε by the combination of a Drude term and two Lorentz oscillators:

$$\varepsilon(\omega) = \varepsilon_\infty - \frac{\omega_{\mathrm{pu}}^2}{\omega^2 - i\Gamma_D\omega} + \sum_{j=1}^{2} \frac{f_j\omega_{0j}^2}{\omega_{0j}^2 - \omega^2 + i\gamma_j\omega}. \quad (2)$$

In Eq. (1), ε_∞ is equal or larger than unity to compensate for the contribution of higher-energy transitions that are not taken into account by the Lorentz terms. The Drude term is characterized by the unscreened plasma energy $\hbar\omega_{\mathrm{pu}}$ and the damping factor Γ_D. The Lorentz oscillators are located at energy position $\hbar\omega_{0j}$, with strength f_j and damping factor γ_j.

Figure 2 shows a typical example of the dielectric function of a thin TiN film, which was deposited in 220 cycles onto a thermal oxide substrate prepared at 750 °C. The dielectric function of the thin TiN film was extracted from the data by the Drude-Lorentz parametrization. Both the real (ε_1) and imaginary (ε_2) parts of the dielectric function are shown and the contributions of the Drude and Lorentz oscillators are indicated. Due to the near-infrared extension up to a wavelength of 1700 nm, a large part of the Drude oscillator is probed and, therefore, the Drude term can be fitted with high accuracy.

From the Drude oscillator parameters, material parameters such as the conduction electron density [Eq. (1)], the mean free path (MFP) of the conducting electrons, the resistivity (ρ), and mass density (ρ_m) can be calculated according to the free-electron model:[19]

$$\mathrm{MFP} = \hbar\left[\frac{3\pi^2\varepsilon_0}{(m^*e)^2}\right]^{1/3}\frac{\omega_{\mathrm{pu}}^{2/3}}{\Gamma_D}, \quad (3)$$

$$\rho = \left(\frac{1}{\varepsilon_0}\right)\frac{\Gamma_D}{\omega_{\mathrm{pu}}^2}, \quad (4)$$

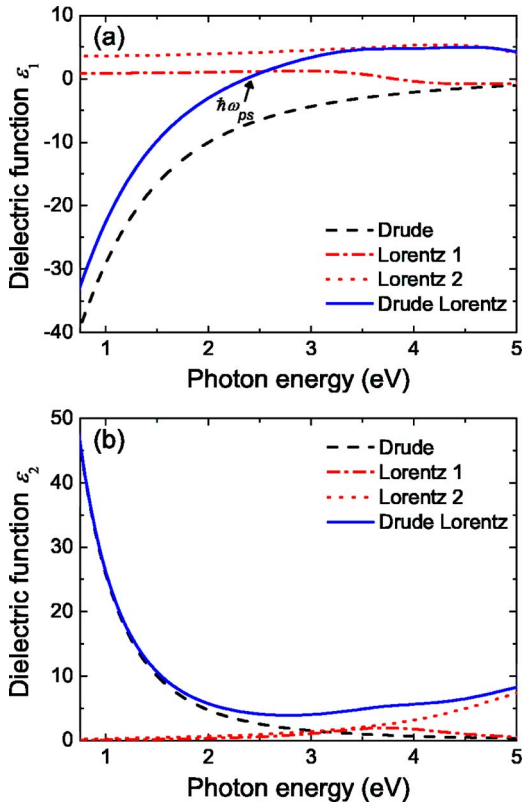

FIG. 2. (Color online) (a) The real (ε_1) and (b) the imaginary (ε_2) part of the dielectric function for an 11.7 nm thick TiN film deposited at 400 °C as obtained from the spectroscopic ellipsometry data using the Drude-Lorentz parametrization. The separate contributions of the Drude and two Lorentz oscillators to the dielectric functions are indicated.

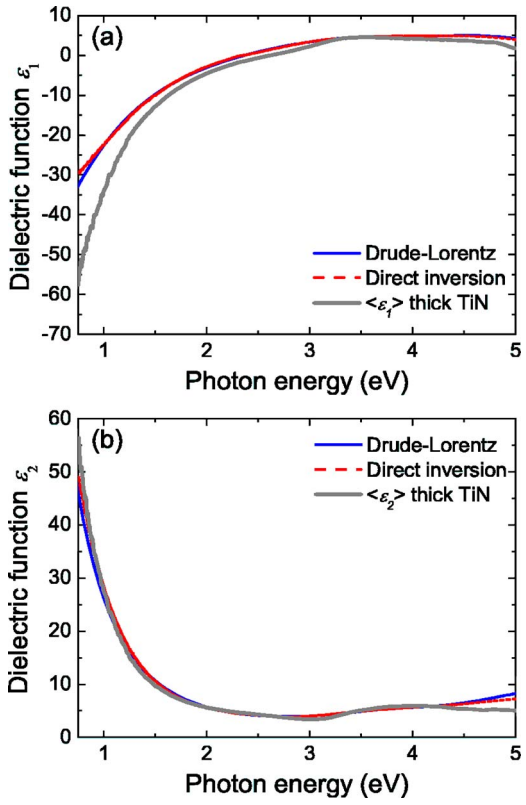

FIG. 3. (Color online)(a) The real (ε_1) and (b) the imaginary (ε_2) part of the dielectric function of an 11.7 nm thick TiN film deposited at 400 °C as obtained from the spectroscopic ellipsometry data using the Drude-Lorentz parametrization and the direct numerical inversion method. The dielectric functions are compared to the pseudodielectric functions $\langle\varepsilon_1\rangle$ and $\langle\varepsilon_2\rangle$ of a nearly opaque 65 nm thick TiN film.

$$\rho_m = \left(\frac{\varepsilon_0 m^* A}{e^2 N_0 Z}\right)\omega_{\mathrm{pu}}^2, \tag{5}$$

where N_0 is the number of Avogadro, Z is the number of conduction electrons per atom, and A is the atomic mass of the material, respectively. For TiN, the atomic mass is A $(=A_{\mathrm{Ti}}+A_{\mathrm{N}})=62$ amu and we assume a value of $Z=0.95$.[21] An estimation on the effective electron mass is required to calculate the mass density. Following Patsalas and Logothetidis, we estimate the effective electron mass to be $m^*=1.15m_e$, in which m_e is the electron rest mass.[21]

The Lorentz oscillators can be used to obtain insight into the stoichiometry of the TiN film. In literature, it is reported that the stoichiometry of the films can be related to the screened plasma energy.[29,30] In contrast to the unscreened plasma energy which is defined for an ideal metal (only a Drude oscillator), the screened plasma energy ($\hbar\omega_{\mathrm{ps}}$) is introduced for a nonideal metal with interband transitions related to absorptions by bound electrons. The screened plasma energy is defined by the energy position where the real part of the dielectric function of the nonideal metal is zero (cf. Fig. 2). The strength and position of the Lorentz oscillators will mainly affect the screened plasma energy and, thereby, give insight into the film stoichiometry. However, it must be noted that the Lorentz oscillator fitting is often not unique resulting in a relatively large uncertainty in the Lorentz fit parameters.

2. Direct numerical inversion

The dielectric function of the TiN film can also be extracted directly from the pseudodielectric function of the total sample by the method of direct numerical inversion.[31] Assuming that the substrate properties are not affected by the deposition, trial spectra of ε_1 and ε_2 can be obtained by a wavelength point-to-point exact numerical inversion using trial film thicknesses. This procedure is repeated for several trial thicknesses and it is decided upon the correct film thickness from the criterion that the ε_1 and ε_2 spectra should be smooth and show no unphysical artifacts such as strange (oscillatory) features. Here, the method of direct numerical inversion was used to examine whether the Drude-Lorentz parametrization is adequate to model the very thin TiN films. Figure 3 shows a comparison of the dielectric functions obtained from both model approaches applied to the same data used in Fig. 2. It is seen that the dielectric functions of both the model approaches overlap very well in a large photon energy region. The TiN film thicknesses obtained from the Drude-Lorentz parametrization and the direct numerical inversion method result in consistent thicknesses of 11.7 ± 0.5 and 11 ± 1 nm, respectively. Furthermore, it is observed that both methods show good agreement for film thicknesses down to 3 nm, as is reported elsewhere.[32]

The pseudodielectric function of a 65 nm thick TiN film is also plotted in Fig. 3. The pseudodielectric function of this thick film is approximately equal to the bulk TiN dielectric

TABLE I. Typical Drude-Lorentz oscillator model parameters for a thin and a thick (nearly opaque) TiN film deposited by PA-ALD at 400 °C. The unscreened plasma energy $\hbar\omega_{pu}$ and the Drude broadening Γ_D are given for the Drude term. The oscillator strength f_i, position $\hbar\omega_{0i}$, and broadening γ_i are shown for the two Lorentz oscillators and the offset energy ε_∞ takes higher-energy terms into account. The values reported by Patsalas and Lodothetidis for dc magnetron sputtered TiN films (thickness of 10–100 nm) are shown for comparison (Ref. 21).

	12 nm PA-ALD TiN	65 nm PA-ALD TiN	10–100 nm magnetron sputtered TiN
Drude			
$\hbar\omega_{pu}$ (eV)	7.22±0.05	7.29±0.02	5.7–7.8
Γ_D (eV)	0.86±0.05	0.61±0.01	0.3–1.1
Lorentz			
f_1 (eV)	0.8±0.2	0.2±0.1	0.1–0.6
$\hbar\omega_{01}$ (eV)	3.8±0.1	3.6±0.1	3.62–3.68
γ_1 (eV)	1.6±0.1	0.7±0.1	0.7–1.0
f_2 (eV)	3.5±0.3	5.8±0.1	1.5–5.8
$\hbar\omega_{02}$ (eV)	5.6±0.1	6.4±0.1	5.2–6.3
γ_2 (eV)	2.3±0.3	4.7±0.2	2.3–3.8
ε_∞ (eV)	3.0±0.1	1.5±0.1	Not reported

function because the film is nearly opaque. Figure 3 shows that the dielectric function of the thin TiN film has a good overlap with the pseudodielectric function of the thick TiN film. A slight discrepancy between the dielectric functions of the thin and thick TiN is, however, observed at higher photon energies. The influence of a surface roughness layer on the dielectric function of the thin film was simulated, but could not account for the observed difference. Most likely, the discrepancy can be explained by slight change in TiN material properties during growth (see Sec. IV), which might shift the Lorentz oscillator to a higher photon energy.

From a careful examination, it was found that the film thickness deduced does not depend critically on the specific material properties used. This has the important implication that the film thickness as a function of PA-ALD cycles can be accurately determined using the fit parameters that are optimized for the final film thickness. This approach makes the data analysis less laborious than having to optimize the complete set of model parameters to extract film thickness for each *in situ* measurement. Typical Drude-Lorentz fit parameters for a thin and thick TiN film are presented in Table I. These values are compared to values obtained from the literature and a good agreement in Drude-Lorentz fit parameters is found with the results obtained by Patsalas and Logothetidis, who used dc reactive magnetron sputtering and an additional substrate bias to deposit their TiN films.[21] In particular, the Drude term is well defined due to the dominant contribution in the dielectric function (cf. Fig. 2). The fit procedure was therefore mainly focused on this Drude term which is also used to calculate the material parameters of the TiN film. The results obtained are compared to *ex situ* analysis in the next section.

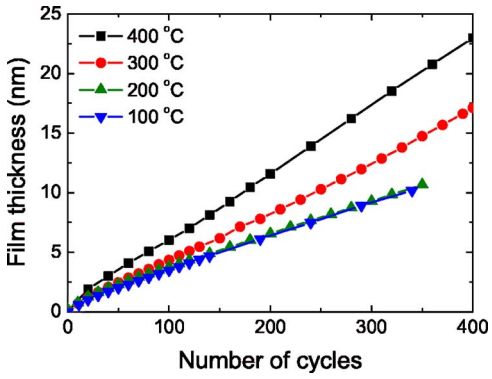

FIG. 4. (Color online)Thickness of TiN films as a function of number of PA-ALD cycles as obtained by *in situ* spectroscopic ellipsometry. The films were deposited on native oxide covered *c*-Si substrates for substrate temperatures between 100 and 400 °C.

IV. RESULTS AND DISCUSSION

A. Material properties of ultrathin TiN films determined by *in situ* SE

1. Physical properties TiN films

Spectroscopic ellipsometry is used to monitor the PA-ALD of TiN for different deposition temperatures (100–400 °C) on native oxide covered silicon substrates. The TiN film thickness as a function of PA-ALD cycles is shown in Fig. 4. The material properties calculated from the *in situ* ellipsometry data are shown in Table II for the films ranging in thickness between 10 and 23 nm. Figure 4 shows that the film thickness is linear with the number of ALD cycles for the full range of deposition temperatures investigated, apart from a nucleation region (<50 cycles) for initial film growth (see Sec. IV B). The growth rate of the PA-ALD process is given by the slope of the growth curves for the linear growth region (cf. Table II) and it is observed that the growth rate per cycle increases with increasing deposition temperature. Such an increase in growth rate with deposition temperature was also reported by others for similar ALD processes.[33,34]

Ex situ XRR measurements were carried out to measure the film thickness for TiN films deposited at H-terminated *c*-Si substrates; however, the films were deposited with a different number of cycles compared to the films listed in Table II. Therefore, the growth rate obtained from both techniques will be compared. The growth rates calculated from the XRR measurements are 0.062±0.002, 0.035±0.002, 0.027±0.002, and 0.026±0.002 nm/cycle for depositions at 400, 300, 200, and 100 °C, respectively, which is in fair agreement with the growth rate obtained by SE.

Atomic force microscopy data in Table II show that the deposited films have a low surface roughness which is comparable to the surface roughness (~0.3 nm) of the substrate itself. On the basis of this low surface roughness, as expected for the layer-by-layer growth by ALD, we conclude that the films are sufficiently smooth to omit a surface roughness layer in the optical model used for SE data analysis.

RBS analysis showed that the TiN films are (nearly) stoichiometric ([N]/[Ti]=1.0±0.1) with only a small Cl and O impurity content. This shows that good quality TiN films can be deposited by PA-ALD even at low substrate temperature while it also validates the SE data analysis based on the Drude-Lorentz parametrization for TiN. The film stoichiometry is also deduced from the SE analysis by the determina-

TABLE II. Material properties of thin TiN films deposited on native oxide covered *c* Si substrates at different substrate temperatures. Using the Drude-Lorentz parametrization, the film thickness, growth rate, conduction electron density, electron mean free path (MFP), resistivity, and mass density are calculated from the *in situ* ellipsometry data. The resistivity and electron MFP are given at deposition temperature and at room temperature (in between parentheses). The accuracy of the data fit is expressed by the mean squared error (MSE) of the fit. Atomic force microscopy is used to determine the surface roughness, while the stoichiometry and impurity content are determined by Rutherford backscattering spectroscopy. The first column gives the typical absolute errors in the parameters unless indicated otherwise.

	Deposition temperature			
	400 °C	300 °C	200 °C	100 °C
MSE of fit	16	16	18	95
Film thickness (nm)	23.0±0.5	17.1	10.7	10.2±1
Growth rate (nm/cycle)	0.057±0.001	0.044	0.028	0.028±0.003
Conduction electron density N (10^{22} cm^{-3})	4.4±0.1	4.3	4.3	4.6±0.3
Electron mean free path (MFP) (nm)	0.72 (0.90)±0.05	0.73 (0.86)	0.59 (0.68)	0.32 (0.36)±0.2
Resistivity ρ ($\mu\Omega$ cm)	142 (121)±10	142 (126)	176 (166)	315 (310)±40
Mass density ρ_m (g cm^{-3})[a]	4.7±0.1	4.7	4.6	5.0±0.4
Surface roughness (nm)	0.5±0.1	0.5	0.3	0.4
Stoichiometry [N]/[Ti]	1.0±0.05	0.91	0.95	1.0
Cl content (at. %)	0.3±0.2	0.4	1	7
O content (at. %)	1.6±0.2	2.8	1.4	4.4

[a]Assuming that the effective mass $m^*=1.15m_e$ as reported in Ref. 21.

tion of the screened plasma energy. We found that the screened plasma energy of the deposited films does not depend on deposition temperature and the value of $\hbar\omega_{ps}=2.3\pm0.1$ eV corresponds to a slightly overstoichiometric TiN_x ($x=1.1$) film.[29,30] Considering the uncertainty in this method, this is in fair agreement with the results obtained by RBS analysis.

The mass density calculated from *in situ* SE can be compared with *ex situ* XRR data for two thick TiN films that were deposited at 100 and 400 °C in order to obtain a sufficient sensitivity in the XRR mass density. For a 45 nm thick TiN deposited at 100 °C mass densities of 3.9±0.1 and 3.7±0.1 g/cm^{-3} were obtained from the SE and XRR data, respectively. For a 65 nm thick TiN deposited at 400 °C, the SE and XRR measurements resulted in 4.8±0.1 and 4.9±0.1 g cm^{-3}, respectively. These values for the mass density are somewhat lower than the literature value for bulk TiN (5.21 g cm^{-3}),[35] but the values are similar to densities of thin TiN films reported in the literature.[9,21]

2. Electronic properties of TiN films

The electronic properties of the TiN films are directly calculated from the *in situ* SE data using the Drude-Lorentz parametrization. However, the electronic properties of the TiN film depend on substrate temperature due to electron-phonon scattering.[36] Therefore, to make a correct comparison between the electronic properties of the films deposited at different temperatures, these properties should be determined at the same substrate temperature. To do so, the temperature coefficient of the electronic properties was determined and used to correct the *in situ* data obtained at the specific deposition temperature to room temperature.

A TiN film was deposited at a substrate temperature of 400 °C and *in situ* SE was used to monitor the change in the Drude fit parameters as a function of substrate temperature during the cooling down of the sample to room temperature. It was observed that only the Drude broadening varied with temperature and that the unscreened plasma energy remained approximately constant. The resistivity, electron MFP, and conduction electron density were calculated from the data and are shown in Fig. 5 as a function of substrate temperature. The resistivity increases and electron MFP decreases linearly with increasing substrate temperature as caused by a more pronounced electron-phonon scattering at higher substrate temperature. Electron-phonon scattering should have no influence on conduction electron density, which is validated by the temperature independent conduction electron density observed in Fig. 5(b). The calculated temperature coefficient of resistivity (TCR) for TiN of 5.5×10^{-4} K^{-1} is in good agreement with the TCR values of 6×10^{-4} K^{-1} (Ref. 37) and $(1.9-8.3)\times10^{-4}$ K^{-1} (Ref. 38) reported for TiN in the literature.

The resistivity values determined by *in situ* SE for the films deposited at different substrate temperatures were corrected to room temperature and are compared to *ex situ* FPP measurements in Fig. 6(a). The figure shows that the resistivity of the TiN films decreases with increasing deposition temperature. A good agreement is observed between the *in situ* SE and *ex situ* FPP data for substrate temperatures between 200 and 400 °C. The larger difference observed for 100 °C can possibly be attributed to postprocess oxidation[39] of the 100 °C TiN film which has a lower mass density (as clearly suggested by the 45 nm thick film) and a higher O impurity content (cf. Table II). Furthermore, from the data we can draw the important conclusion that our PA-ALD technique results in low resistivity TiN films, even at 100 °C deposition temperature as compared with results reported in the literature.[7,34,40]

The electrical resistivity of a metallic film is inversely proportional to both the electron MFP and the conduction

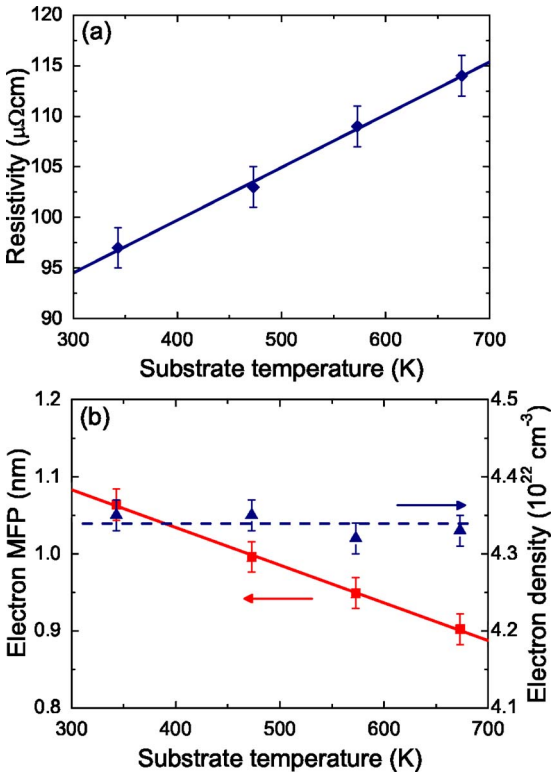

FIG. 5. (Color online) The intrinsic temperature dependence of (a) the resistivity, and (b) the electron mean free path (MFP) and the conduction electron density. The data were obtained for a TiN film deposited at 400 °C by monitoring the film by ellipsometry during the cooling down process from 400 to 100 °C. For the resistivity and electron mean free path, the solid lines are fits to the data which are used to extrapolate the *in situ* data to room temperature. The dashed line for the conduction electron density is a guide to the eye.

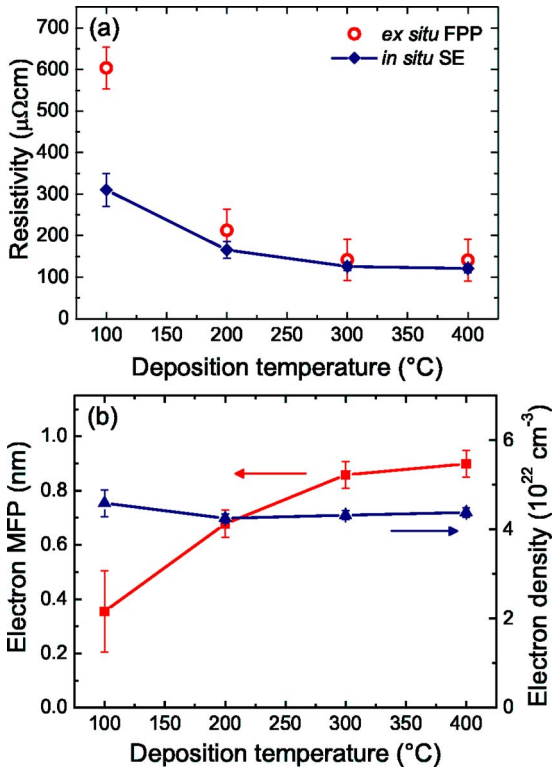

FIG. 6. (Color online) (a) The room temperature values of the resistivity, determined by *in situ* spectroscopic ellipsometry and *ex situ*-four point probe analysis, and (b) the electron mean free path (MFP) and the conduction electron density as a function of deposition temperature. The data obtained at a certain deposition temperature were converted to room temperature values using the relations presented in Fig. 5.

electron density. Therefore the trend of the resistivity in Fig. 6(a) can be understood in more detail by considering these properties which were also calculated from the *in situ* SE data and which are shown in Fig. 6(b). The figure shows that the electron MFP increases with deposition temperature, while the conduction electron density remains virtually constant. The observed increase in resistivity for lower deposition temperature in Fig. 6(a) can therefore be attributed to the decrease in electron MFP.

The electron MFP can be compared to the grain size which was determined from XRD analysis on the 45 nm thick TiN film deposited at 100 °C. The XRD analysis showed that the TiN film contained elliptical grains with a height and lateral width of 10 and 6 nm, respectively. Assuming that films initially grow by the coalescence of nucleation sites, we estimate that a thinner TiN film will have a smaller grain height, but a similar value of the lateral grain size. This estimation is substantiated by Li *et al.*, who determined the grain size of a thin TiN film. They reported a lateral grain size of 4 nm for 6 nm thin TiN films deposited by dc reactive magnetron sputtering.[14] Consequently, the observed electron MFP of the TiN films deposited at 100 °C is an order of magnitude smaller than the grain size determined with XRD. Therefore it can be concluded that the electron MFP is not limited by the grain size of the TiN film but by the presence of point defects and impurities in the film (cf. Table II). Especially the increasing Cl impurity level shows a clear correlation with the decreasing electron mean free path in the film, as shown in Fig. 6(b).

B. Issues related to ultrathin TiN film growth

In the previous section it was shown that information on important material properties of the TiN films can be obtained by *in situ* SE and that the results are in good agreement with those obtained from *ex situ* analysis techniques. In this section *in situ* SE will be used to get a more detailed understanding of film growth by PA-ALD. Three important issues of ultrathin film growth will be addressed, i.e., size effects in ultrathin metallic films, nucleation for films deposited by ALD, and interface layer formation during the PA-ALD growth process.

1. Size effects

In situ SE is used to monitor the change in electrical properties of TiN as a function of the film thickness for a film deposited at 400 °C. The complete Drude-Lorentz oscillator model is optimized for various film thicknesses and from the optimized fit parameters, the resistivity is calculated as a function of film thickness. Figure 7(a) shows that the resistivity is increasing for decreasing film thickness revealing a clear thickness dependence of the electrical properties of the TiN. The resistivity of the 65 nm thick film of $65 \pm 10\ \mu\Omega\,\mathrm{cm}$ is in good agreement with the resistivity

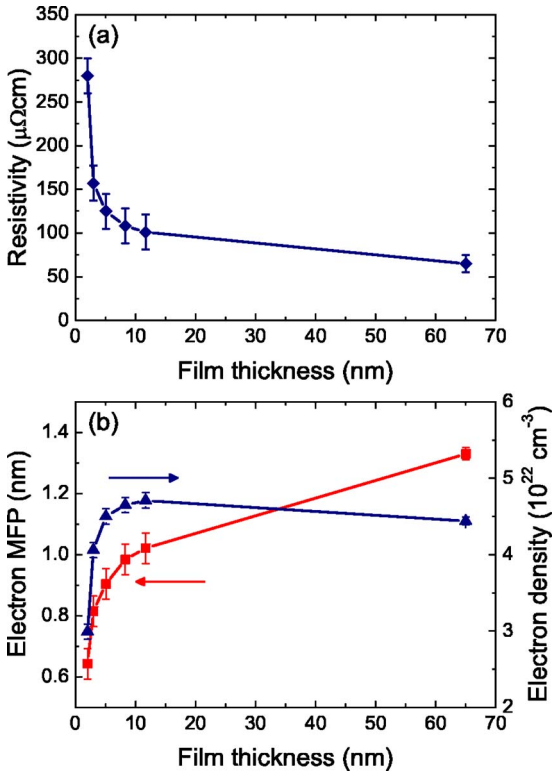

FIG. 7. (Color online) (a) The resistivity, and (b) the electron mean free path (MFP) and the conduction electron density as a function of film thickness monitored by *in situ* spectroscopic ellipsometry. The film was deposited at 400 °C and the data were converted to represent room temperature values.

value of 71 ± 10 $\mu\Omega$ cm determined by *ex situ* FPP.

The electron MFP and conduction electron density were also calculated as a function of film thickness and are shown in Fig. 7(b). The electron MFP decreases with decreasing film thickness, while the conduction electron density is constant down to a film thickness of 5 nm and decreases when going to even a thinner film. The decrease in electron MFP with decreasing film thickness is the result of a more pronounced contribution of electron-sidewall scattering which starts to dominate the electron MFP for the ultrathin films.[8,41] In principle, electron-sidewall scattering always has a contribution to the total of scattering mechanisms in the film, but can be neglected for thick films. Figure 7(b) therefore clearly reveals that size effects are strongly influencing the material properties for ultrathin films and that these size effects can be investigated by *in situ* SE.

2. Film nucleation

The high sensitivity of SE in combination with the ALD technique is an excellent tool to study the nucleation of thin films on differently prepared substrates. To this end, TiN films were deposited at a substrate temperature of 400 °C on different thermal oxides prepared by the procedures described in Sec. II. During the nucleation phase, *in situ* SE data are obtained after each PA-ALD cycle and Fig. 8 shows the TiN thickness as a function of the number of ALD cycles. A distinction in nucleation behavior on the different thermal oxides is observed, as can clearly be seen from the inset of Fig. 8. All films show a nucleation delay after which the

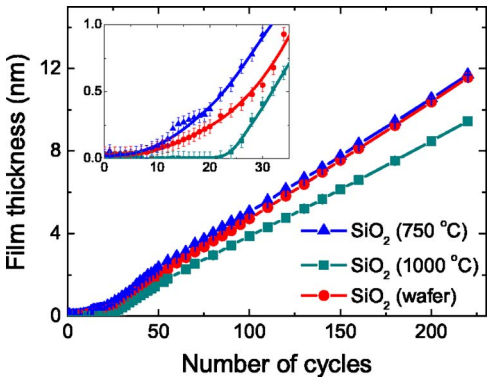

FIG. 8. (Color online) The thickness of TiN films grown on different thermal SiO_2 substrates monitored by *in situ* spectroscopic ellipsometry and shown as a function of number of PA-ALD cycles. The inset displays the initial growth region in more detail. Two substrates were prepared by the method of calcination and preheated at temperatures of 750 and 1000 °C, the other substrate was an as-received wafer with 410 nm thermal oxide.

growth rate increases when the surface becomes completely covered with TiN nucleation sites. Figure 8 shows that at a film thickness of approximately 2 nm, film closure is obtained and the growth rate becomes constant as is expected for ALD growth. The difference in nucleation delay can be related to the number of reactive surface groups on the initial thermal oxide surface.[16,24,42] The surface of thermal oxide mainly consists of siloxane bridges and only some hydroxyl groups are present depending on the preheat temperature of the oxide (750 °C: 1–2 OH nm^{-2}, 1000 °C: 0–0.5 OH nm^{-2}).[24,42] Because the $TiCl_4$ precursor molecules can only react with the surface hydroxyls to form nucleation sites, the most distinct nucleation delay is observed for the thermal oxide preheated at 1000 °C. Satta *et al.* observed a similar nucleation delay on thermal oxide substrates using Rutherford backscattering spectroscopy.[9] A slight difference in growth rate after nucleation on different substrate material was also reported by Satta *et al.*,[9] but the underlying mechanism is still unclear.

3. Interface layer formation

Another issue related to the application of the (plasma-assisted) ALD technique is the possible modification of the substrate by interface layer formation during growth. *In situ* SE can also be applied to study this effect as revealed by an experiment in which a TiN film is deposited on a H-terminated *c*-Si substrate, while the growth is monitored by *in situ* SE. To fit the SE data, the two-layer SE model was extended with an additional layer to model the formation of an interface layer of SiN_x in between the *c*-Si substrate and TiN film as also supported by *ex situ* RBS and XPS measurements. The dielectric function of the interfacial SiN_x was modeled by means of a standard Cauchy dispersion relation,[17] and the TiN and SiN_x thicknesses were fitted as a function of the number of PA-ALD cycles. Figure 9 shows the resulting change in thickness of both the TiN and SiN_x films. Prior to the TiN film growth, the formation of the SiN_x layer is observed, which can be explained by the exposure of the substrate to the H_2/N_2 plasma. Subsequently, the TiN film nucleates on the SiN_x surface. Figure 9 shows that the

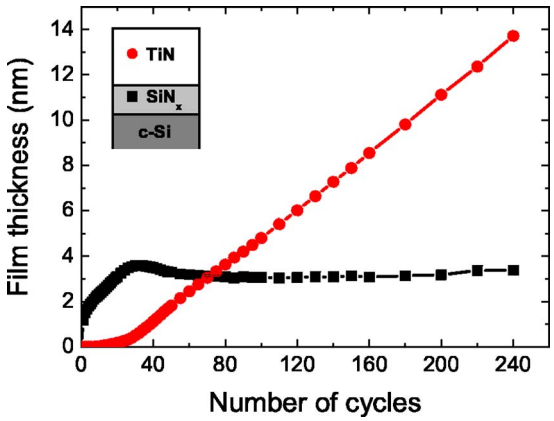

FIG. 9. (Color online) The thickness of a TiN film deposited by plasma-assisted atomic layer deposition on a H-terminated *c*-Si substrate shown as a function of the number of PA-ALD cycles. The inset shows the model used to analyze the *in situ* ellipsometry data. The change in thickness of a SiN_x interface layer formed during the PA-ALD process is also given.

interfacial film thickness finally saturates to a thickness of 3.4 nm. The interface layer thickness determined from the SE data is close to the interface thickness determined by XPS (~2.5 nm) and RBS analyses (~3 nm).

In the literature, it is reported that $TiCl_4$ molecules do not react with silicon hydrides on a crystalline silicon surface.[43] As a consequence, the film nucleation is very slow on H-terminated *c*-Si, because the $TiCl_4$ molecules can only nucleate on surface defects.[16] The plasma-induced formation of the SiN_x film creates surface groups such as NH_x groups that are reactive to the $TiCl_4$ molecules and facilitates the film nucleation. The formation of an interfacial layer during (PA-)ALD is also observed for the growth of HfO_2 (Refs. 44–46) and Al_2O_3 (Refs. 15 and 47) but the use of *in situ* SE to monitor the interface formation during ALD has not been reported yet.

V. CONCLUSIONS

The growth process of ultrathin TiN films by the plasma-assisted atomic layer deposition technique was monitored by *in situ* spectroscopic ellipsometry with a photon energy range of 0.75–5 eV. Adopting the Drude-Lorentz oscillator parametrization to describe the dielectric function of the TiN films, the film thickness and material properties were determined from the *in situ* ellipsometry data. The dielectric function of the thin TiN films and the film thickness obtained by the Drude-Lorentz parametrization showed good agreement with the dielectric function and film thickness obtained by the method of direct numerical inversion and with the bulk dielectric function of a (nearly) opaque TiN film. Furthermore, it was verified that the thickness and material properties of the thin TiN films determined by *in situ* spectroscopic ellipsometry were in good agreement with the results obtained by *ex situ* film analysis such as x-ray reflectometry and four-point probe measurements.

Because electronic properties such as conduction electron density, electron mean free path, and electrical resistivity can directly be obtained from the *in situ* ellipsometry data, the variation in resistivity of the TiN films with deposition temperature could be related to the change in electron mean free path in the films caused by a deposition temperature dependent impurity level in the films. Moreover, by acquiring *in situ* spectroscopic ellipsometry data during TiN film growth, several aspects related to thin film properties were addressed. The electrical resistivity of the films increased with decreasing film thickness (2–65 nm) and this so-called finite size effect is caused by a more pronounced electron-sidewall scattering for decreasing film thickness leading to a reduced electron mean free path. A distinct difference in nucleation delay on different thermal oxide substrates was observed by *in situ* SE, which could be directly related to the difference in density of surface hydroxyls on the substrates. Using ellipsometry to monitor the PA-ALD of TiN on a H-terminated *c*-Si substrate, the formation of an interfacial SiN_x layer was observed before the onset of TiN film growth. It was therefore clearly established that fundamental insight into the growth of ultrathin films by techniques such as ALD can be obtained by monitoring the process with *in situ* spectroscopic ellipsometry.

ACKNOWLEDGMENTS

Dr. P. C. Thune and E. M. E. van de Kimmenade of the Department of Chemical Engineering are thanked for the preparation of the thermal oxide substrates. Part of the *ex situ* analysis was carried out at Philips Research Eindhoven; the RBS analysis by Dr. Y. Tamminga and T. Dao, the XRD measurements by F. Bakker and Dr. H. Wondergem, and the XPS analysis by A. H. C. Hendriks. Dr. A. Rahtu of ASM Microchemistry is acknowledged for the XRR thickness and density calculations. M. J. F. van de Sande, J. Jansen, A. B. M. Hüsken, and H. M. M. de Jong are thanked for their skillful technical assistance. This work was supported by the Dutch Technology Foundation STW. The research of one of the authors (W.K.) was made possible by a fellowship from the Royal Netherlands Academy of Arts and Sciences (KNAW).

[1] T. Suntola, Mater. Sci. Rep. **4**, 261 (1989).
[2] M. Leskelä and M. Ritala, Thin Solid Films **409**, 138 (2002).
[3] M. Ritala and M. Leskelä, in *Handbook of Thin Film Materials*, edited by H. S. Nalwa (Academic, San Diego, CA, 2001), Vol. 1, p. 103.
[4] H. Kim, J. Vac. Sci. Technol. B **21**, 2231 (2003).
[5] K.-E. Elers, J. Winkler, K. Weeks, and S. Marcus, J. Electrochem. Soc. **152**, G589 (2005).
[6] S. B. S. Heil, E. Langereis, A. Kemmeren, F. Roozeboom, M. C. M. van de Sanden, and W. M. M. Kessels, J. Vac. Sci. Technol. A **23**, L5 (2005).
[7] S. B. S. Heil, E. Langereis, M. C. M. van de Sanden, and W. M. M. Kessels (unpublished).
[8] W. Steinhögl, G. Schindler, G. Steinlesberger, M. Traving, and M. Engelhardt, J. Appl. Phys. **97**, 23706 (2005).
[9] A. Satta, A. Vantomme, J. Schuhmacher, C. M. Whelan, V. Sutcliffe, and K. Maex, Appl. Phys. Lett. **84**, 4571 (2004).
[10] Y. Travaly, J. Schuhmacher, A. M. Hoyas, M. Van Hove, K. Maex, T. Abell, V. Sutcliffe, and A. M. Jonas, J. Appl. Phys. **97**, 84316 (2005).
[11] A. Satta *et al.*, Microelectron. Eng. **60**, 59 (2002).
[12] F. Greer, D. Fraser, J. W. Coburn, and D. B. Graves, J. Vac. Sci. Technol. A **21**, 96 (2003).
[13] J. W. Elam, M. Schuisky, J. D. Ferguson, and S. M. George, Thin Solid Films **436**, 145 (2003).
[14] T. Q. Li, S. Noda, F. Okada, and H. Komiyama, J. Vac. Sci. Technol. B **21**, 2512 (2003).
[15] M. M. Frank, Y. J. Chabal, and G. D. Wilk, Appl. Phys. Lett. **82**, 4758 (2003).

[16]S. Haukka, E.-L. Lakomaa, and A. Root, J. Phys. Chem. **97**, 5085 (1993).
[17]H. G. Tompkins and W. A. McGahan, *Spectroscopic Ellipsometry and Reflectrometry* (Wiley, New York, 1999).
[18]B. Sell, A. Sänger, and W. Krautschneider, J. Vac. Sci. Technol. B **21**, 931 (2003).
[19]N. W. Ashcroft and N. D. Mermin, *Solid State Physics* (Saunders College, Orlando, FL, 1976).
[20]F. Wooten, *Optical Properties of Solids* (Academic, New York, 1972).
[21]P. Patsalas and S. Logothetidis, J. Appl. Phys. **90**, 4725 (2001).
[22]P. Patsalas and S. Logothetidis, J. Appl. Phys. **93**, 989 (2003).
[23]H. G. Tompkins and E. A. Irene, *Handbook of Ellipsometry* (William Andrews, Inc., New York, 2005).
[24]L. T. Zhuravlev, Colloids Surf., A **173**, 1 (2000).
[25]G. E. Jellison, Jr. and F. A. Modine, Phys. Rev. B **27**, 7466 (1983).
[26]J. A. Woollam Co., Inc., 650 J Street, Suite 39, Lincoln, NE 68508; http://www.jawoollam.com
[27]B. Karlsson, J.-E. Sundgren, and B.-O. Johansson, Thin Solid Films **87**, 181 (1982).
[28]K. Postava, M. Aoyama, and T. Yamaguchi, Appl. Surf. Sci. **175–176**, 270 (2001).
[29]S. Logothetidis, I. Alexandrou, and A. Papadopoulos, J. Appl. Phys. **77**, 1043 (1995).
[30]J. H. Kang and K. J. Kim, J. Appl. Phys. **86**, 346 (1999).
[31]H. Arwin and D. E. Aspnes, Thin Solid Films **113**, 101 (1984).
[32]E. Langereis, S. B. S. Heil, M. C. M. van de Sanden, and W. M. M. Kessels, Phys. Status Solidi C **2**, 3958 (2005).
[33]J. Kim, H. Hong, S. Ghosh, K.-Y. Oh, and C. Lee, Jpn. J. Appl. Phys., Part 1 **42**, 1375 (2003).
[34]D.-H. Kim, Y. J. Kim, J.-H. Park, and J. H. Kim, Mater. Sci. Eng., C **24**, 289 (2004).
[35]D. R. Lide, *Handbook of Chemistry and Physics*, 85th ed. (CRC, Boca Raton FL, 2005).
[36]N. Kontoleon, K. Papathanasopoulos, K. Chountas, and C. Papastaikoudis, J. Phys. F: Met. Phys. **4**, 2109 (1974).
[37]H. Zafer Durusoy, O. Duyar, A. Aydınlı, and F. Ay, Vacuum **70**, 21 (2003).
[38]J. F. Creemer, P. M. Sarro, M. Laros, H. Schellevis, T. Nathoeni, L. Steenweg, V. Svetchnikov, and H. W. Zandbergen, Proceedings of SAFE 2004, 2004 (unpublished), p. 742.
[39]D.-H. Kim, J. J. Kim, J. W. Park, and J. J. Kim, J. Electrochem. Soc. **143**, L188 (1996).
[40]K. Yokota, K. Nakamura, T. Kasuya, K. Mukai, and M. Ohnishi, J. Phys. D **37**, 1095 (2004).
[41]A. F. Mayadas and M. Shatzkes, Phys. Rev. B **1**, 1382 (1970).
[42]S. Haukka and T. Suntola, Interface Sci. **5**, 119 (1997).
[43]G. C. Abeln, M. C. Hersam, D. S. Thompson, S.-T. Hwang, H. Choi, J. S. Moore, and J. W. Lyding, J. Vac. Sci. Technol. B **16**, 3874 (1998).
[44]Y. Won, S. Park, J. Koo, J. Kim, and H. Jeon, Appl. Phys. Lett. **87**, 262901 (2005).
[45]Y. Senzaki, S. Park, H. Chatham, L. Bartholomew, and W. Nieveen, J. Vac. Sci. Technol. A **22**, 1175 (2004).
[46]P. S. Lysaght, B. Foran, G. Bersuker, P. J. Chen, R. W. Murto, and H. R. Huff, Appl. Phys. Lett. **82**, 1266 (2003).
[47]S.-C. Ha, E. Choi, S.-H. Kim, and J. S. Roh, Thin Solid Films **476**, 252 (2005).